CHAPTER 17

Electron Microscopy of the Amphibian Model Systems *Xenopus laevis* and *Ambystoma mexicanum*

Thomas Kurth[*], Jürgen Berger[†], Michaela Wilsch-Bräuninger[‡], Susanne Kretschmar[*], Robert Cerny[§], Heinz Schwarz[†], Jan Löfberg[¶], Thomas Piendl[#], *and* Hans H. Epperlein[‖]

[*]Center for Regenerative Therapies, TU Dresden, D-01307 Dresden, Germany

[†]Max-Planck Institute of Developmental Biology, D-72076 Tübingen, Germany

[‡]Max-Planck Institute of Molecular Cell Biology and Genetics, D-01307 Dresden, Germany

[§]Department of Zoology, Charles University Prague, CZ-128 44 Prague, Czech Republic

[¶]Section of Animal Development and Genetics, Uppsala University, S-752 36 Uppsala, Sweden

[#]NET-Network for Educational Technology, ETH Zürich, CH-8092 Zürich, Switzerland

[‖]Department of Anatomy, TU Dresden, D-01307 Dresden, Germany

METHODS IN CELL BIOLOGY, VOL. 96

978-0-12-381007-6
DOI: 10.1016/S0091-679X(10)96017-2

Abstract

In this chapter we provide a set of different protocols for the ultrastructural analysis of amphibian (*Xenopus*, axolotl) tissues, mostly of embryonic origin. For *Xenopus* these methods include: (1) embedding gastrulae and tailbud embryos into Spurr's resin for TEM, (2) post-embedding labeling of methacrylate (K4M) and cryosections through adult and embryonic epithelia for correlative LM and TEM, and (3) pre-embedding labeling of embryonic tissues with silver-enhanced nanogold. For the axolotl (*Ambystoma mexicanum*) we present the following methods: (1) SEM of migrating neural crest (NC) cells; (2) SEM and TEM of extracellular matrix (ECM) material; (3) Cryo-SEM of extracellular matrix (ECM) material after cryoimmobilization; and (4) TEM analysis of hyaluronan using high-pressure freezing and HABP labeling. These methods provide exemplary approaches for a variety of questions in the field of amphibian development and regeneration, and focus on cell biological issues that can only be answered with fine structural imaging methods, such as electron microscopy.

I. Introduction

Amphibians are classic model organisms for vertebrates in cell and developmental biology. Urodeles (newts and salamanders, such as *Triturus* and *Ambystoma*) and anurans (frogs and toads, such as *Rana, Bufo, Xenopus*) are the model species studied most intensively since the late 19th century. In the early days of embryology, many studies on developmental processes were performed especially in amphibians. The main advantages of amphibian models are the generation of vast amounts of embryos, the external development, as well as the robustness of the embryos tolerating experimental manipulations, such as tissue grafting (explantation, implantation, or transplantation), even across species. Many important concepts, such as cell fate determination or embryonic induction, were formulated in these times (Hamburger, 1988), mainly based on studies with urodele embryos. Later, the South African clawed frog, *Xenopus laevis*, was introduced as the most important amphibian model, due to practical considerations such as the reliable induction of ovulation by injection of hormones or the easy chemical removal of the jelly coat around the eggs (Sive *et al*., 2000). Over the past 100 years, some of the hallmark experiments in developmental biology were performed with amphibians as model organisms, for example, the "organizer experiment." In this experiment, an area in the future dorsal region of the embryo was defined that, upon transplantation into a host embryo, was able to instruct the formation of a complete secondary body axis from graft and host tissues (Spemann and Mangold, 1924). Further important experiments were the first cloning of a vertebrate by microinjection of nuclei from differentiated cells into enucleated eggs (Gurdon *et al*., 1975), the identification of the first organizer gene, the homeobox gene *goosecoid* (after more than 60 years of frustrating efforts; Cho *et al*., 1991), followed by the

subsequent molecular characterization of the organizer (reviewed in De Robertis, 2009), and recently, the introduction of antisense-Morpholinos for specific gene knock-down in embryos (Heasman *et al*., 2000).

The major disadvantage of *Xenopus laevis* as a model for genetic studies is its pseudotetraploid genome and the long generation time (1–2 years). Therefore, the interest had shifted to other model organisms, such as *Drosophila melanogaster, Caenorhabditis elegans*, or the zebrafish *Danio rerio*. But *Xenopus* laevis and the axolotl, *Ambystoma mexicanum*, persisted as important models in developmental and regeneration biology. In fact, *Xenopus laevis* still is the best-understood model for mesoderm induction and patterning, or the regulation of cell movements in the early gastrulating or neurulating embryo (Heasman, 2006; Keller *et al*., 2003; Kimelman, 2006). Recently, a close relative, *Xenopus tropicalis,* emerged as a new amphibian model organism with a diploid genome and a shorter generation time of 3–6 months (Amaya *et al*., 1998).

In addition, the *Xenopus* egg is a powerful system for biochemical studies using egg extracts (Crane and Ruderman, 2006; Cross and Powers, 2009; Mandato *et al*., 2001; Maresca and Heald, 2006) and for patch-clamp studies of ion-channels that are ectopically expressed in the oocyte membrane (Tammaro *et al*., 2008). The axolotl also continues to be an important model in a variety of research areas, from physiology to development and regeneration (Voss *et al*., 2009).

In the past few years, the regenerative potential of both *Xenopus* and the axolotl has gained increased interest (Slack *et al*., 2008; Voss *et al*., 2009). In this respect, the neoteny of the axolotl is especially remarkable as it allows the animal to regenerate complex body structures, such as limbs, tail, spinal cord, heart, or jaws (e.g., Kragl *et al*., 2009; Mchedlishvili *et al*., 2007; Sobkow *et al*., 2006). Recently, it has become possible to study the genomic background for this regenerative potential (Habermann *et al*., 2004; Putta *et al*., 2004), which opens the door for deeper insights into the underlying processes, especially with respect to possible medical implications, and a potential to stimulate tissue regeneration in humans.

Many of the questions that arise during developmental or regeneration studies finally focus on basic cell biological questions concerning subcellular protein localization, macromolecular dynamics, vesicle trafficking, signaling regulation, etc. Often these cell biological questions can only be answered by using fine structural imaging methods, including electron microscopy.

II. Rationale

Our goal is to provide a set of different methods for the ultrastructural analysis of amphibian tissues, mostly of embryonic origin. The protocols include ultrastructural and immunolabeling approaches for TEM and SEM. In general, embryos are considered as “problematic samples” due to their yolk content, the concentration of very different tissues within a small specimen and, in many cases, the impossibility of dissecting them before fixation. Here, most of the presented methods are modified

standard preparations that help to yield reasonable ultrastructure and/or protein localization. It is well accepted that cryofixation, especially high-pressure freezing (HPF), is currently the method of choice for optimal ultrastructural preservation (Moor, 1987; Studer *et al*., 2001). Unfortunately, both *Xenopus* and axolotl embryos are too big to be high-pressure frozen properly *in toto*, the only possible exception being small explants (see Section III.B). Therefore, most of the protocols presented here still rely on chemical fixation and gelatin or resin embedding.

III. Methods

A. Xenopus

Although *Xenopus* is widely used as a laboratory animal, information on the histology of embryonic stages is rather limited. There is a detailed light microscopical description of tissue sections through early embryos (Hausen and Riebesell, 1991), but later stages, from tailbud stage 27 onward, and the histogenesis of tissues and organs, are poorly documented. The current knowledge about these later events is deduced mainly from low-resolution gene expression patterns (Sive *et al*., 2000). Moreover, EM studies on *Xenopus* embryos are relatively rare and the *Xenopus* Laboratory Manual (Sive *et al*., 2000) does not even contain a paragraph on specimen preparation for EM. However, studies involving EM analysis were performed in many fields of cell and developmental biology, where *X. laevis* and *X. tropicalis* are important vertebrate models. The topics include egg development and early cleavage (e.g., Cardellini *et al*., 2007; Danilchik and Brown, 2008; Danilchik *et al*., 2003; Fesenko *et al*., 2000; Kalt, 1971; Merzdorf *et al*., 1998; Müller and Hausen, 1995), gastrulation (e.g., Hardin and Keller, 1988; Keller, 1980, 1981; Kurth and Hausen, 2000; Kurth *et al*., 1999; Nakatsuji *et al*., 1985; Reintsch and Hausen, 2001; Shook *et al*., 2004; Winklbauer and Nagel, 1991; Winklbauer *et al*., 1992), neurulation and neural crest (NC) cell migration (e.g., De Calisto *et al*., 2005; Sadaghiani and Thiebaud, 1987; Schroeder, 1970; Youn and Malacinski, 1981), and organogenesis (Giacomello *et al*., 2002; Moriya *et al*., 2000; Osafune *et al*., 2002; Youn and Malacinski, 1981; Youn *et al*., 1980). Most of these studies include SEM observations, but rarely TEM or immuno-EM.

In addition to studies on embryonic development, several cell biological EM studies on the cytoskeleton or nuclear structures were performed with *Xenopus* as a model organism (e.g., Allen *et al*., 2007a, b; Gajewski and Krohne, 1999; Lourim and Krohne, 1993; Schwab *et al*., 1998; Stick and Schwarz, 1983; Coughlin *et al*., 2007; Goldberg *et al*., 2008; Walther, 2008). The 3D structure of the nuclear pore complex (NPC), for example, was elucidated using *Xenopus* NPCs (Akey and Radermacher, 1993; Maco *et al*., 2006; Stoffler *et al*., 2003).

The focus of current *Xenopus* research lies on the genetic control of early development (axis determination, mesoderm induction and patterning, mesoderm and NC cell movements) or organogenesis (somitogenesis, NC derivatives, formation of organ

anlagen), which is studied in embryos ranging from cleaving to tailbud stages (De Robertis, 2009; Heasman, 2006; Kimelman, 2006).

In this paragraph, we describe a standard embedding protocol for the ultrastructural analysis of embryos as well as pre- and post-embedding immunolabeling protocols for adult and embryonic tissues.

1. Embedding of Gastrula and Tailbud Embryos into Spurr's Resin for TEM

Cells of early *Xenopus* embryos are "filled" with yolk platelets that contain lipo-glyco-phosphoprotein crystals (Hausen and Riebesell, 1991). This material is difficult to fix, infiltrate, and cut properly (Kalt and Tandler, 1971; Kurth, 2003). To balance extraction, infiltration efficiency, and cutting properties with ultrastructural preservation, the following protocol is used: fixation with a glutaraldehyde–paraformaldehyde-(GA/PFA)-mixture modified after Karnovsky (1965) and embedding in Spurr's low-viscosity resin (Spurr, 1969).

Embryos are kept in modified Barth's solution (MBSH, Fey and Hausen, 1990) and staged according to Nieuwkoop and Faber (1967). Embryos are fixed at least overnight at 4°C in modified Karnovsky's fixative (2.5% GA, 2% PFA in 50 mM HEPES, pH 7.4). After several washes (6 × 10 min in 100 mM HEPES, 2 × 10 min in PBS) samples are embedded in 3% low-melting-point agarose. The agarose block is trimmed asymmetrically to a trapezoid pyramid, which allows orientation of the sample at a later stage during embedding into Spurr's resin. Agarose blocks enclosing the specimens are then postfixed with 1% OsO_4/PBS on ice for at least 4 h to overnight, followed by washes in PBS (5 × 5 min) and water (4 × 5 min), *en bloc* contrasting in 1% aqueous uranyl acetate (2 h on ice) and washes in water (4 × 5 min). Dehydration occurs in a graded series of ethanol in water (30, 50, 70, 90, 96%, 30 min each) with two final steps in water-free ethanol (100% ethanol on a molecular sieve, 30 min each). Subsequently, the samples are infiltrated in mixtures of Spurr's and water-free ethanol (1:2; 1:1; 2:1), 1.5 h each, and finally in pure Spurr's resin for 2 h and overnight. The blocks are embedded in flat embedding molds (EMS), oriented, and cured in an oven at 65°C overnight. Ultrathin sections are contrasted with lead citrate and uranyl acetate after Venable and Coggeshall (1965).

The ultrastructure of *Xenopus* embryos prepared in that way is shown in Fig. 1. The amphibian blastula is surrounded by an outer layer of polarized epithelial cells (Müller and Hausen, 1995). This so-called primary epithelium is the first cell population displaying signs of differentiation. At the beginning of gastrulation, a subpopulation of these outer epithelial cells, at the border of vegetal mass and marginal zone, undergoes apical constriction, thereby acquiring a typical flask-like shape (Figs. 1A and B; Hardin and Keller, 1988; Keller, 1981). This process involves both the actin cytoskeleton and microtubules (Lee and Harland, 2007). At the ultrastructural level, these so-called bottle cells are characterized by apical villi-like surface extensions (Figs. 1B and C), an electron-dense subapical layer, vesicles underneath the apical cell surface, and accumulated pigment granules (Figs. 1B and C). Later on, bottle cells respread and form part of the anterior pharynx epithelium

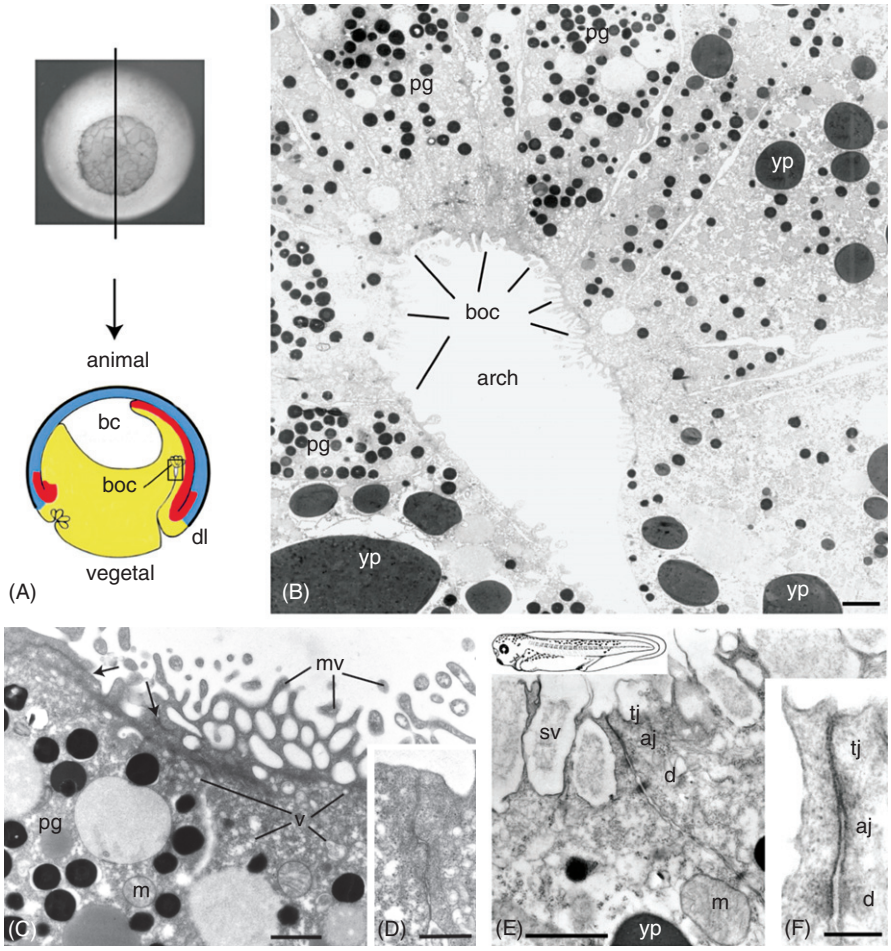

Fig. 1 Ultrathin Epon sections through *Xenopus* gastrula (stage 11, A–D) and tailbud (stage 37, E, F) embryos. (A) Vegetal view of the blastopore (top) and schematic of a median section (bottom, sectioning plane indicated by the black line in the embryo on top). Constricted epithelial cells (bottle cells, boc) are indicated; bc, blastocoel; dl, dorsal lip. The square indicates the region displayed in (B). (B) Apical, constricted parts of several bottle cells at the tip of the archenteron (arch) with accumulated pigment granules (pg). (C) Cellular details of bottle cells: microvilli (mv), subapical vesicles (v), pigment granules, and junctions between the cells (arrows). (D) Typical bottle cell contact at higher magnification. (E) Epidermal cells of a stage 37 tailbud embryo with a junctional complex: tight junction (tj), adherens junction (aj), desmosome (d). m, mitochondrium; sv, secretory vesicle; yp, yolk platelet. (F) Junctional complex at higher magnification. Scale bars: B, 2 µm, C,E, 1 µm, D, 0.5 µm, F, 0.2 µm. (See Plate no. 20 in the Color Plate Section.)

(Keller, 1981). Apical junctions are visible between bottle cells (arrows in Fig. 1C). However, a clear distinction of tight junctions, adherens junctions, and desmosomes, as shown in the outer epithelium of a stage 37 tailbud embryo (Figs. 1E and F), is often not possible.

2. Post-embedding Labeling of Methacrylate Sections (K4M) and Cryosections Through Adult and Embryonic Epithelia for Correlative Light and Electron Microscopy (CLEM)

On-section or post-embedding labeling of resin or cryosections is a powerful method for light and electron microscopy, yielding both ultrastructural and immunolabeling information (Schwarz and Humbel, 2007; Slot and Geuze, 2007). The major disadvantage of this method is its relatively low labeling efficiency, which is often critical in the early amphibian embryo (Kurth, 2003).

a. Fixation Tissue blocks not larger than 1 mm^3 are dissected in 2% PFA in 0.1 M phosphate buffer (PB), transferred immediately into 4% PFA/PB or 4% PFA/ 0.1% GA/PB, and fixed at least overnight at 4°C.

b. Progressive Low Temperature (PLT)-Embedding into K4M and Sectioning Specimens are transferred to 4-ml glass vials with screw caps or 0.5-ml Eppendorf microtubes, washed for 5 × 5 min in PB, and dehydrated in a graded series of ethanol/water: 30%, 50% (20 min each at room temperature), 70% (30 min at 4°C), 80% and 90% (30 min each at −20°C), 96% and 2 × 100% (at −35°C, 1 h each). Infiltration occurs at −35°C in Lowicryl K4M/ethanol mixtures (1:2, 1:1, 2:1) for 1 h each, followed by two steps in pure K4M for 2 h and overnight. The samples are then polymerized by UV light at −35°C for 24 h (e.g., in a Leica AFS2). For immunofluorescence, 200-nm-thick sections are collected from the water trough with a perfect loop, mounted on polylysine-coated microscope slides, and encircled with a water-repellent silicon pen. Ultrathin sections (50–70 nm) are collected on 50–100 mesh grids for immunogold labeling.

c. Embedding into Gelatin/Sucrose and Cryosectioning after Tokuyasu Fixed samples are washed for 5 × 5 min in PB, infiltrated stepwise with 2% gelatin (10 min at room temperature), 5, 10% (10 min each at 37°C), and cooled down on ice. Blocks (1.5 × 1.5 mm future cutting surface or smaller) are cut on ice and transferred to 2.3 M sucrose in water for at least overnight at 4°C. Sucrose-infiltrated blocks are mounted on specimen carriers (pins) and plunge-frozen in liquid nitrogen. Specimens can be stored either in sucrose solution or in LN_2 for at least several months. Semi-thin sections (300 nm) are picked up in methyl cellulose sucrose (MCS, 1 part 2% MC + 1 part 2.3 M sucrose) and mounted on polylysine-coated microscope slides. Ultrathin sections (70 nm) are picked up in MCS and transferred with a perfect loop to 50 mesh copper grids. Sections can be stored at 4°C in a humid chamber until staining (Griffith and Posthuma, 2002).

d. Correlative Fluorescence- and Immunogold-Labeling of K4M-Sections Resin sections are "rehydrated" for 2 × 5 min in PBS, blocked with 0.2% gelatin + 0.5% BSA in PBS (PBG, 2 × 10 min), and incubated with primary antibody

(approximately 1–10 µg/ml) for 30 min to 2 h. All antibody/protein A gold solutions are centrifuged before application (5000 U/min for 5 min). After washes in PBG (6 × 3 min) sections are incubated with secondary antibody (e.g., fluorophore-labeled or gold-conjugated antibodies, protein A gold) for 30 min to 2 h. For fluorescence, sections are washed for 6 × 3 min in PBS, counterstained with DAPI (0.4 µg/ml) for 5 min, washed for 2 × 3 min in PBS, and mounted with Mowiol/DABCO or ProLong Gold. For EM, gold-labeled sections are washed for 6 × 3 min in PBG, 2 × 3 min in PBS, and 5 × 2 min in distilled water, before being contrasted with 1–2% aqueous uranyl acetate for 5 min. After final short washes in distilled water the sections dried and ready for investigation. If desired, lead citrate staining can be performed according to Venable and Coggeshall (1965).

e. Correlative Fluorescence- and Immunogold-Labeling of Cryosections For fluorescence microscopy the sections are washed for 2 × 5 min with PBS to get rid of the sucrose and 4 × 5 min (at 37°C) and 5 × 3 min (at room temperature) with PBS to melt and remove the gelatin. Sections are permeabilized with 0.1% Tween 20 in PBS for 5 min, washed with PBS (5 × 2 min), blocked with 0.1% glycin/PBS (2 × 3 min) and 1% BSA/PBS (2 × 5 min), and incubated with primary antibody (approximately 1–10 µg/ml in BSA/PBS, 30 min – 1 h). Sections are washed with BSA/PBS (5 × 2 min), incubated with fluorophore-labeled antibodies (Alexa-conjugated: 1:200, Cy3-conjugated: 1:400; from here on sections have to be protected from light) in BSA/PBS for 30 min to 1 h, washed in PBS (5 × 3 min), counterstained with DAPI (see above), washed (2 × 3 min PBS), and mounted with ProLong Gold.

For EM the grids are put upside down on 2% phosphate-buffered gelatin in a 3-cm petri dish. The gelatin is melted under a lamp (approximately 40°C), transferred to a 37°C-incubator for 20 min, washed with 0.1% glycin/PBS (5 × 1 min), blocked with 1% BSA/PBS (2 × 5 min), and incubated with primary antibody for 30 min to 1 h. After washing in PBS (4 × 2 min), the sections are incubated with gold-labeled secondary antibodies or Protein A gold (30 min-1 h), in PBS (3 × 5s, 4 × 2 min), stabilized with 1% glutaraldehyde (5 min), and washed extensively with distilled water (10 × 1 min) to get rid of the phosphates. With mouse IgGs as primary antibodies, and Prot A gold as marker, a bridging rabbit anti-mouse antibody is used because Prot A does not bind mouse IgGs. Then, sections are stained with neutral uranyl oxalate (2% UA in 0.15 M oxalic acid pH 7.0) for 5 min, washed for a short time in water, and incubated in methyl cellulose uranyl acetate (9 parts 2% MC + 1 part 4% UA pH 4) on ice for 5 min. The uranyl oxalate step is optional. It stabilizes membrane lipids and enhances the contrast in some cases (Griffiths *et al.*, 1984; Tokuyasu, 1976). Finally, grids are looped out and the MC/UA film is reduced to an even and thin film and air dried.

The examples shown in Figs. 2A–C (K4M sections) and Figs. 2 D and E (cryosections) show adult *Xenopus* enterocytes stained with anti-β-catenin (P14L, Schneider *et al.*, 1996). The protein is localized in the basolateral membrane and concentrated in adherens junctions. Since on-section-labeling is highly dependent on the copy number of a given protein, it is in many cases not sensitive enough for labeling embryonic

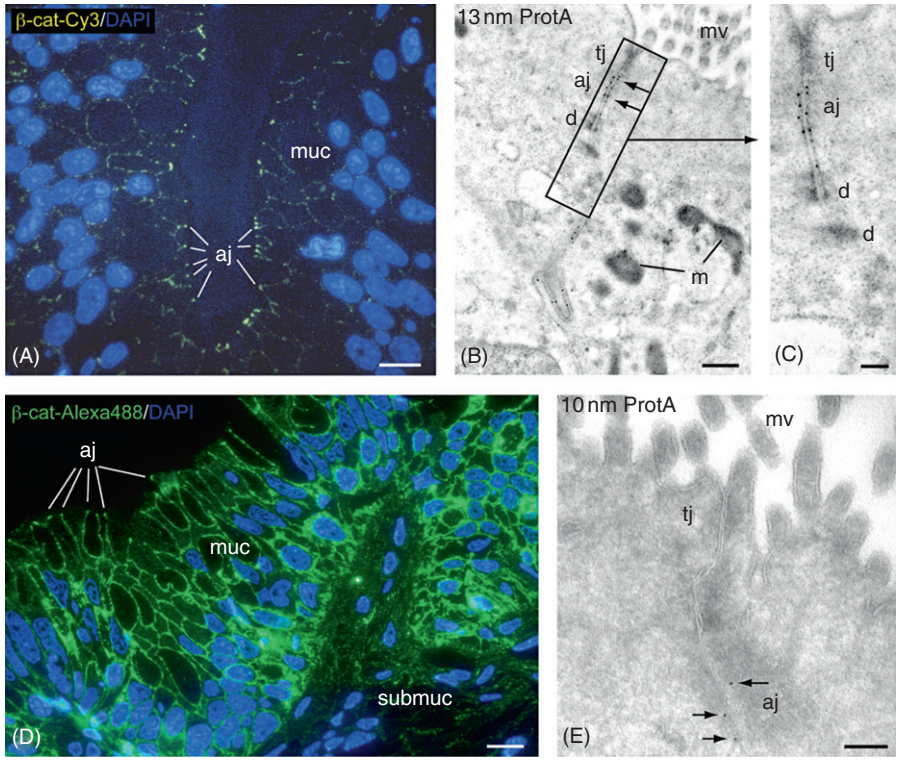

Fig. 2 Correlative on-section labeling of thin K4M sections (A–C) and cryosections (D,E) through mucosal (muc) and submucosal (submuc) layers of the adult *Xenopus* intestine. Sections are stained with anti-β-catenin and fluorescent secondary antibodies or Protein A Gold as indicated. For fluorescence, sections were counterstained with DAPI. The signal is visible in the basolateral membrane domains especially in the adherens junctions (aj); d, desmosome; m, mitochondrium; mv, microvilli; tj, tight junction. Scale bars: A and D, 10 μm; B, 0.5 μm, C and E, 200 nm. (See Plate no. 21 in the Color Plate Section.)

tissues (not shown). The staining is usually stronger in cryosections, which, therefore, might be a promising alternative for embryologists. In Fig. 3, junctions are labeled in cryosections through the epidermis of tails in tailbud embryos. As a proof of principle, the tight junction marker ZO-1 (mouse monoclonal ZO-1-1A12, Invitrogen) and β-catenin are shown. Many developmental biologists focus their interest on early embryos, such as blastula, gastrula, or neurula stages, where many important developmental decisions are made. As mentioned earlier, these embryos, however, are extremely difficult to cut properly because of their high yolk content.

3. Pre-Embedding Labeling of Embryonic Tissues using Silver-Enhanced Nanogold

For the early embryo, an alternative labeling method is needed when post-embedding labeling of resin sections is not sensitive enough and cryosections are difficult to obtain.

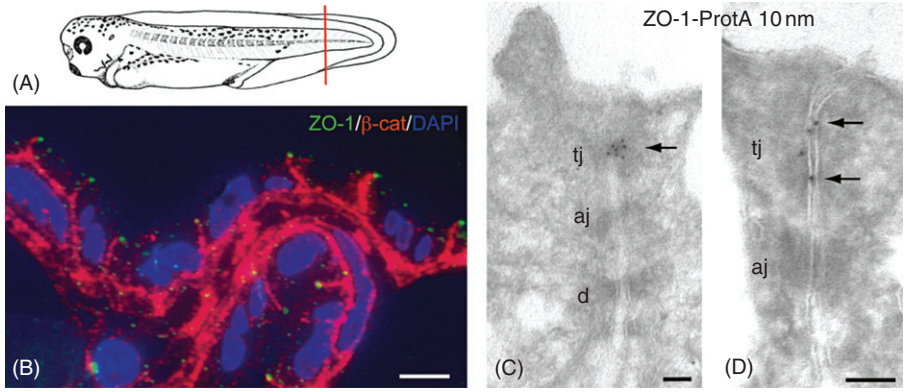

Fig. 3 Correlative on section-labeling of cryo-sections through a stage 37 *Xenopus* embryo. (A) Embryo with the sectioning plane indicated. Immunofluorescence (B) and immunogold-labeling (C,D) of thin cryosections through the epidermis stained with anti-β-catenin (+ goat-anti-rabbit-Alexa555) and anti ZO-1 (+ goat-anti-mouse Alexa488, B) or with anti-ZO-1 followed by Protein A 10 nm gold (C,D). Anti-ZO-1 marks the tight junctions (tj) between the epithelial cells; aj, adherens junction; d, desmosome. Scale bars: B, 5 μm, C and D, 100 nm. (See Plate no. 22 in the Color Plate Section.)

In such cases, we use a pre-embedding approach with silver-enhanced nanogold markers (Fig. 4; Kurth, 2003).

a. Fixation and Preparation of Vibratome Sections Embryos are fixed as described in paragraph b, washed in 100 mM HEPES (6 × 5 min) and PBS (2 × 5 min), and embedded in 2% low-melting-point agarose in PBS. Sections (50 μm) are cut with a vibrating razor blade on a vibratome (e.g., Vibratome series 1000, Pelco, speed 2.5, amplitudes 6–7).

b. Antibody Labeling The sections are blocked with 20% normal goat serum (NGS) in PBS containing 0.1% saponin for permeabilization (2 h at room temperature) and incubated with primary antibodies diluted in 20% NGS/PBS/0.05% saponin for at least overnight at 4°C. After washes in PBS (short, 5, 10, 15, 30 min, 2 × 1 h, 1 × 2 h), nanogold-conjugated antibodies (Fab-fragments, e.g., Aurion/EMS) are applied overnight at 4°C, the sections are washed in PBS (short, 5, 10, 15, 30 min, 2 × 1 h, 1 × 2 h), postfixed in 2% glutaraldehyde/PBS (1 h at room temperature), and again washed in PBS (5 × 5 min).

c. Silver Enhancement After washes in water (4 × 5 min), to get rid of the phosphates, silver enhancement is performed after Danscher (1981; See also Lah *et al.*, 1990; Stierhof, 2009) in the dark for 30 min to 1 h. Alternatively, the R-Gent silver enhancement Kit from EMS/Aurion can be used. After enhancement the specimens are washed in water (4 × 5 min), postfixed in 1% aqueous uranyl acetate for 1h on ice, and washed again for 4 × 5 min in water.

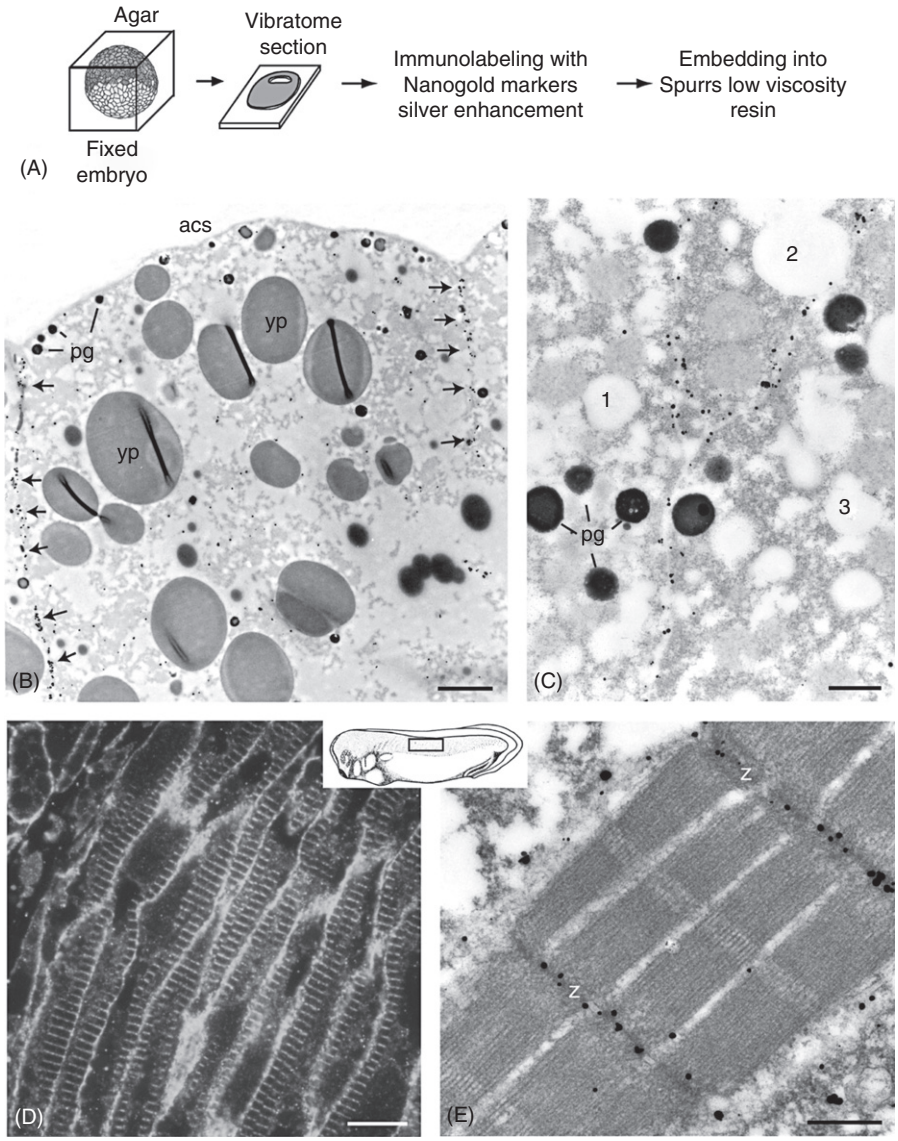

Fig. 4 Pre-embedding labeling of β-catenin in *Xenopus* embryos using nanogold and silver enhancement. (A) Schematic drawing of the procedure. (B) Animal cap cell of a blastula (stage 7) with β-catenin in the basolateral membrane (arrows); acs, apical cell surface; pg, pigment granules; yp, yolk platelet. (C) In the deeper layers the protein is expressed in all membrane contacts between cells (1–3). (D,E) Indirect correlative labeling of sagittal vibratome sections through the myotome of a tailbud embryo (stage 30). (D) Fluorescent staining of β-catenin in a striped pattern (anti-β-catenin, Goat-anti-rabbit-Cy3). (E) Labeling of the Z-disks at the EM level (Z), vibratome section embedded in Spurr's resin. Scale bars: B, 2 μm; C and E 0.5 μm; D, 20 μm.

d. Dehydration and Embedding The samples are dehydrated in a graded series of ethanol/water (30, 50, 70, 80, 90, 96%, 2× 100% ethanol, 20 min each), and samples are infiltrated in Spurr's low-viscosity resin via a graded series of Spurr–ethanol mixtures (1:2, 1:1, 2:1; 1–2 h each) followed by incubation in pure Spurr's resin for 2 h and overnight. The flat-embedding is done between two foils in a slide-embedding mold. The upper foils can be fixed with two to three small coins. One must be careful at this stage as early embryos are extremely brittle and can easily be destroyed, therefore excess pressure must not be applied. Polymerization occurs at 65°C. Later, the specimens are cut out and mounted on an Epon dummy block for sectioning. Sections can be contrasted with uranyl acetate and lead citrate, as described above.

e. Immunofluorescence In parallel, adjacent vibratome sections can be processed for immunofluorescence. Here the sections are stained with fluorophore-labeled secondary antibodies, postfixed in 4% PFA/PBS, dehydrated in a graded series of ethanol, and flat-embedded in either Technovit 7100 or in Spurr's resin. Technovit can be sectioned 1 μm thin, Spurr even thinner, resulting in high-resolution fluorescence (Kurth, 2003; Kurth *et al*., 1996). Alternatively, silver-enhanced nanogold can be visualized by polarized light on semi-thin sections (Kurth, 2003).

The localization of β-catenin in the basolateral membranes of animal cap cells (blastula embryo, stage 7) is demonstrated (Figs. 4A–C). The protein can also be found in the Z-discs of growing myofibers in the myotome of stage 30 embryos (Figs. 4 D and E). Z-disc localization of β-catenin has been described also for adult heart and skeletal muscle (Kurth *et al*., 1996).

B. Axolotl

Important issues studied with EM in axolotl include spermatogenesis (*TEM*; Miltner and Armstrong, 1983), somite segmentation (*SEM*; Armstrong and Graveson, 1988), pronephric duct migration (*SEM*; Gillespie *et al*., 1985; Zackson and Steinberg, 1987), pigment cell migration and development, neural crest (NC) migration, and extracellular matrix (ECM) organization (*TEM, SEM*; Cerny *et al*., 2004; Epperlein and Löfberg, 1990; Epperlein *et al*., 1997, 2000a, 2000b, 2007; Falck *et al*., 2002; Löfberg *et al*., 1985, 1989a). For the staging of axolotl embryos and larvae up to stage 45, the normal table of Bordzilovskaya *et al*. (1989) is used. The development of limbs, the buds of which start to protrude at stage 40, can be staged from stage 45 onward in a special table (Nye *et al*., 2003). In this section, EM protocols for SEM and TEM preparations and TEM immunohistochemistry will be presented. They focus on NC cell migration and ECM organization during development, key topics of research in axolotl and other vertebrates.

Axolotl embryos are much larger, but otherwise similar to *Xenopus* embryos. Thus, when transferring the methods applied in *Xenopus* to axolotl, the large size of these embryos has to be considered. In addition, different topics were studied in the axolotl field and a somewhat different set of EM-preparation protocols has been developed.

1. SEM Analysis of Migrating Neural Crest Cells

In axolotl embryos, from which the epidermis is removed, premigratory and migrating neural crest (NC) cells can vaguely be visualized with LM, but very well with SEM. The NC is formed during neurulation. Prospective NC cells are contained in the apical parts of the neural folds bordering either side of the neural plate. After the neural folds have converged dorsally and fused into the neural tube, NC cells leave the association of neural tube cells and lie on top of the neural tube. On the cranial neural tube the NC forms a flat epithelium whereas on the trunk tube it is organized as a narrow, multilayered cell string (Fig. 5). These embryos were fixed in modified Karnovsky's fixative (2.5% GA and 2% PFA in 0.1 M phosphate buffer, pH 7.5, 4°C), followed by a washing step in buffer and postfixation in 1% OsO_4 in 0.1 M potassium–phosphate buffer, pH 7.5, 4°C (for details see Cerny *et al.*, 2004; Epperlein and Löfberg, 1990). From their site of origin on top of the neural tube, NC cells migrate out into different body sites on stereotyped routes through an ECM-rich environment and give rise to a wide variety of derivatives (Hall and Hörstadius, 1988; Le Douarin and Kalcheim, 1999). In the head, NC cells form several discrete and coherent cell streams. These originate from specific hindbrain levels of the NC and are directed laterally (Fig. 5A). In the trunk, NC cells do not form streams but migrate out laterally as single cells (Fig. 5C) between somites and epidermis, and medially between somites and the neural tube. Lateral NC cells give rise to pigment cells and medial ones form neurons and glia of the peripheral nervous system.

a. Tissue Preparation and Fixation of Embryos for SEM Analysis of NC Cells Embryos are kept in Steinberg solution (Steinberg, 1957) either at room temperature or at 7–8°C to slow down embryonic development. To partially remove the epidermis and expose areas of interest, embryos are transferred into an agar dish filled with cold Steinberg solution (7–8°C). The epidermis is removed with tungsten needles and the embryos are then transferred into modified Karnovsky's fixative in 0.1 M potassium–phosphate buffer (pH 7.5, 4°C) and kept at 4°C overnight. Following washes in PBS (30 min, three changes), fixed embryos are transferred to 1% OsO_4 in 0.1 M potassium–phosphate buffer (pH 7.5, 4°C), and kept overnight at 4°C. Then the embryos are washed in PBS and dehydrated through a graded series of ethanol in water: 30, 50% (30 min each at room temperature), 70% overnight at 4°C, 85%, 96%, 3× 100% ethanol (30–60 min each at room temperature). The slow dehydration process helps to prevent the formation of cracks on the surface of the specimen or in the yolk platelets. Subsequently, critical-point drying with liquid CO_2 is performed using a Polaron critical-point dryer. The exchange of ethanol and liquid CO_2 should happen slowly for at least 2–3 h. Finally, the specimens are sputter-coated with gold–palladium and observed with SEM (Fig. 5A, cranial NC; Fig. 5B, trunk NC).

2. SEM and TEM Analysis of Extracellular Matrix (ECM) Material

The ECM consists of proteoglycans, glycoproteins, and glycosaminoglycans, such as hyaluronan. It includes all secreted molecules outside the cells, insoluble fibrils (like

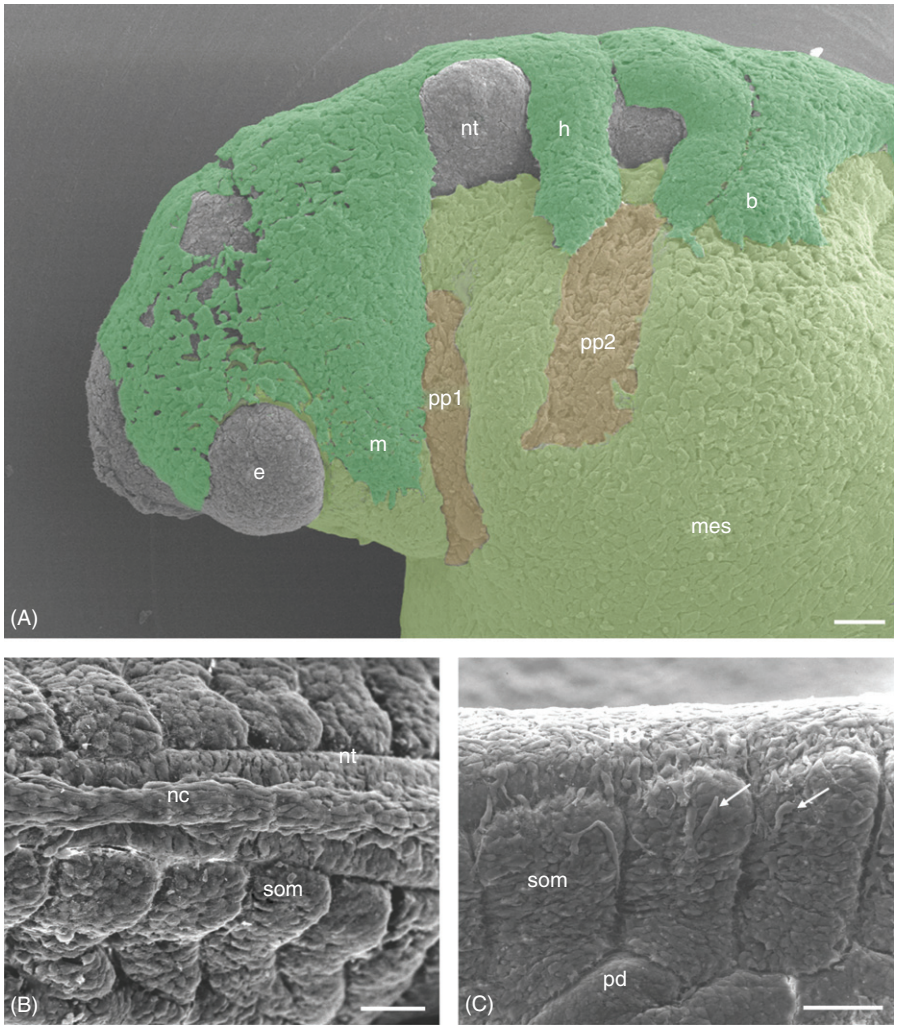

Fig. 5 SEM of axolotl neural crest (NC). (A) Cranial NC streams of an epidermis-free axolotl embryo (stage 25) migrating out laterally on head mesoderm (mes). Prospective pharyngeal pouches (pp 1 and pp 2); mandibular NC stream (m), forming the upper and lower jaw; hyoid NC stream (h), forming the hyoid; common branchial NC stream (b) segregating into NC streams 3–6 later. e, eye; nt, neural tube. (B,C) Midrunk NC. (B) premigratory NC (stage 30/31); NC string (nc) on top of the trunk neural tube (nt). (C) migratory NC (stage 33); single NC cells (arrows) migrate out laterally over the dorsolateral neural tube toward the upper margin of the somites (som). pd, pronephric duct. Scale bars: A, 100 µm, B and C, 50 µm. (See Plate no. 23 in the Color Plate Section.)

collagen or fibronectin), or highly hydrated soluble polymers (like hyaluronan and proteoglycans). The ECM regulates the development and function of almost all cells in metazoan organisms (Reichardt, 1993). In particular, subepidermal ECM from dark

(D/-) axolotl embryos was shown to stimulate NC cell migration in the white (d/d) mutant (Löfberg *et al*., 1985, 1989a,b). Our knowledge of the ultrastructure of the ECM is very limited and even artifacts have been published. During standard chemical fixation (modified Karnovsky: 2.5% GA and 2% PFA in 0.1 M phosphate buffer) and the following dehydration steps, water is extracted from the ECM, which results in shrinkage and structural damage. For example, wide spaces become visible between fibrocytes in the dorsal fin of axolotl larvae observed in the SEM, and the cells seem to lie in an empty environment (Epperlein *et al*., 1997). Precipitates of the ECM are retained as fibrillar networks between the cells and on their surfaces. By contrast, living fibrocytes, studied in the confocal microscope, are embedded in their natural interstitial ECM (Epperlein *et al*., 1997). Here the cells appear voluminous, send out branching cell processes, and lie in an amorphous extracellular ground substance with interspersed fibrils. In order to find components of the ECM that specifically stimulate lateral NC (pigment) cell migration in the wild-type (dark, D/d) axolotl embryo or inhibit this migration in the white mutant (d/d), detailed investigations on ECM components between dark and white embryos were carried out. Differences could be observed in the distribution of collagen type III (Perris *et al*., 1990) and keratan sulfate (Olsson *et al*., 1996a). Functional tests with collagen type III, however, could not show any influences on pigment cell distribution (Olsson *et al*., 1996b), and the effect of keratan sulfate is still unknown. Furthermore, the analysis of the distribution of hyaluronan (HA) did not reveal differences in dark or white embryos (Epperlein *et al*., 2000a). The ultrastructure of HA is particularly difficult to demonstrate. Because of its hydration HA resists standard chemical fixation and can only be shown with difficulty, even after cryofixation (see below). More recently, the TGF-β growth factor BMP-4 was shown to exert an inhibitory effect on pigment cell (melanophore) distribution in dark embryos whereas Noggin, its antagonist, could stimulate melanophore migration in the white mutant (Hess *et al*., 2008).

b. Tissue Preparation and Chemical Fixation for SEM and TEM Analysis of ECM To demonstrate ECM material in the SEM or TEM, standard chemical fixation is insufficient. Reagents like ruthenium red (RR) (Luft, 1971a, b) have to be added to the fixative in order to precipitate ECM components and enhance their contrast. The preparation and fixation (including RR) of embryos is as follows: Embryos are fixed in modified Karnovsky's fixative containing 1.5% GA +1.5% PFA in 0.1 M phosphate buffer (pH 7.4) for at least several hours at 4°C, rinsed in PBS, and postfixed in 1% OsO4 in 0.1 M cacodylate buffer for 4 h. During part of the fixation time (Karnovsky: 30 min, OsO_4: 4 h) both fixatives contain 500 ppm RR. Alternatively, 0.05% tannic acid can be added to Karnovsky's fixative only. After several washes in cacodylate buffer, the specimens are dehydrated in a graded series of ethanol, critical-point dried, and sputtered with gold palladium (SEM; Löfberg *et al*., 1985; see Section 2a), or infiltrated with Epon for ultrathin sectioning (TEM; Löfberg *et al*., 1985). Sections are stained with lead citrate and uranyl actetate as described above, Section IIIA).

Subepidermal ECM of an axolotl embryo (stage 34) fixed with Karnovsky's fixative + RR is shown in Fig. 6A (SEM) and Fig. 6B (TEM). ECM precipitated on a

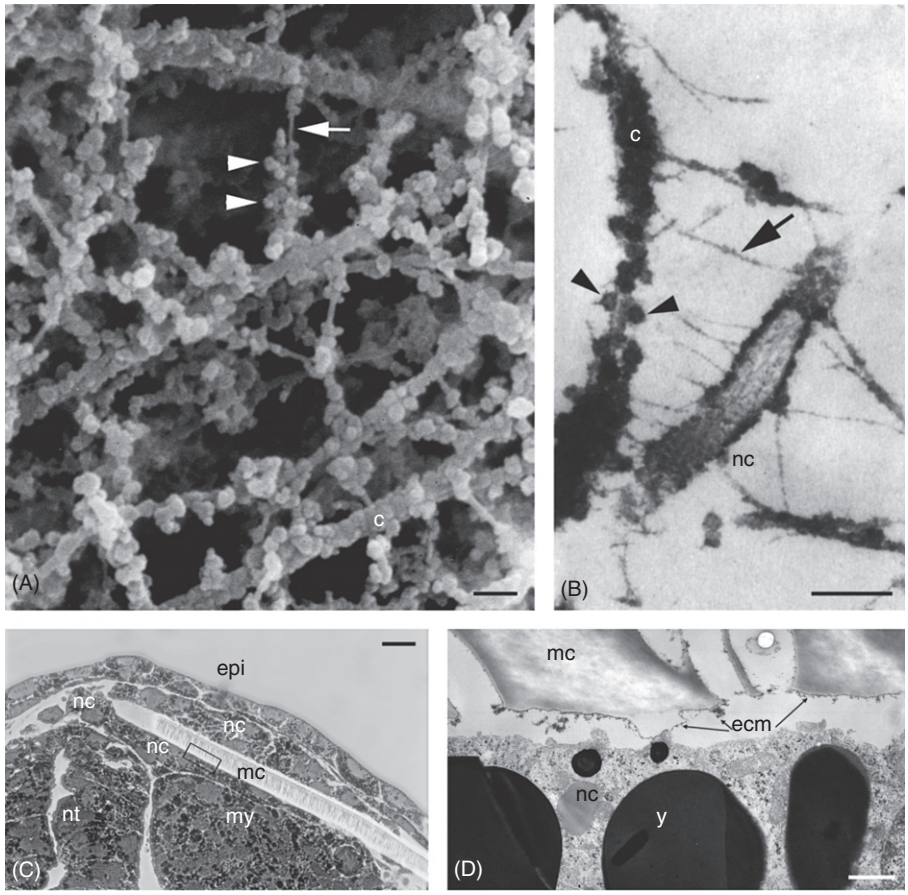

Fig. 6 Subepidermal ECM in the electron microscope. SEM (A) and TEM (B) micrographs of subepidermal ECM from the dorsolateral trunk of axolotl embryos (stage 34) after fixation with Karnovsky's fixative including RR. The thicker fibrils consist of collagen (c), the thinner filaments (arrows) consisting very likely of hyaluronan. Both are decorated with granular precipitates, possibly proteoglycans (arrowheads). RR enhances the preservation of thin filaments and ECM precipitates. In B part of a NC cell (nc) is visible and contacted by matrix filaments and fibrils (C,D) Stimulation of trunk neural crest cell migration in wild-type (dark; D/d) axolotl embryos with dark subepidermal ECM. (C) LM micrograph showing transverse section through the midtrunk region of a wild-type embryo (stage 30) containing a grafted microcarrier (mc, Nuclepore filter) conditioned with ECM of a dark donor embryo. (D) TEM micrograph showing an enlarged contact area (inset in C) between the microcarrier (mc) and a host NC cell whose lateral migration was stimulated by adsorbed dark ECM. ECM material (ecm, arrows) is precipitated following fixation with Karnovsky's fixative containing RR; epi, epidermis; nt, neural tube; my, myotome; ecm, extracellular matrix; y, yolk platelet. Bars: A and B, 0.2 μm, C, 25 μm, D, 0.1 μm. A and B reprinted with permission from Löfberg *et al*. (1989b).

microcarrier using Karnovsky+RR is shown in Figs. 6C and D. Microcarriers (0.1×0.5 mm) cut from Nuclepore filter material (Nuclepore Inc.) were implanted into the dorsolateral trunk of dark (D/-) axolotl embryos (stage 25) with their matt side facing the subepidermal ECM. For adsorbing "dark" ECM, microcarriers were left in the embryo for about 20 h (until stage 30), then they were implanted into dark (D/d) or white (d/d) stage 25 hosts and stayed there until stage 30, where they could stimulate lateral migration of host NC cells (Löfberg *et al*., 1985).

3. Cryo-SEM Analysis of Extracellular Matrix (ECM) Material After Cryofixation

An alternative to chemical fixation is ultrarapid freezing. Several methods of cryofixation, such as plunge-freezing, metal mirror freezing, and high-pressure freezing (HPF), have been introduced over the past decades (Moor, 1987). Tissues that are difficult to fix by conventional means particularly benefit from rapid freezing (i.e., encapsulated tissues, plants, and tissues with a high content of water, such as cartilage; see several chapters of this volume). Therefore, cryofixation is a promising option for the analysis of ECM material.

a. Tissue Preparation and Cryofixation for Cryo-SEM Analysis of ECM Epidermal grafts from the dorsolateral trunk of dark (D/d) anesthetized (MS 222, Sandoz) larvae (stage 40) are transferred into an agar dish containing Steinberg solution (Steinberg, 1957) and quickly arrested between the two halves of a lockable double grid (precleaned by sonication in ethanol/acetone) to prevent curling. The matrix side of the graft has to face the side with the grid slot. The grid containing the epidermal graft is directly plunge-frozen in liquid ethane (plunge velocity 2 m/s), mounted on a cryoholder (Gatan Inc., Pittsburgh, PA) and freeze-dried in a Balzers' MED 010 device (pressure 6.7×10^{-7}mbar; 3 h at −110°C, 1 h at −100°C). Sputter-coating with 3-nm tungsten at the same temperature follows and then the samples are cooled down to −168°C, transferred to the cryo-SEM, and imaged at −168°C (Epperlein *et al*., 1997).

Subepidermal ECM in epidermal grafts from axolotl larvae (stage 40), fixed in modified Karnovsky solution with the addition of CPC (See section IV), followed by plunge-freezing and freeze-drying, shows only unsatisfactory results in the cryo-SEM. The ECM fibrils, consisting mainly of collagen, form a random network with large empty spaces. The fibrils are decorated with only a few, small granular precipitates, which are probably proteoglycans (Fig. 7A). Better structural preservation is obtained by cryofixation (plunge-freezing and freeze-drying). When observed in the cryo-SEM, the ECM fibrils form a dense and relatively even matrix that contains many small clefts and some larger holes. The fibrils are densely covered with precipitates (Fig. 7B).

4. TEM Analysis of the ECM Component Hyaluronan by Cryofixation and HABP Labeling

Hyaluronan (HA) is an extracellular and cell-surface-associated polysaccharide (Toole, 2004). It belongs to the family of glycosaminoglycans (GAGs) that consist

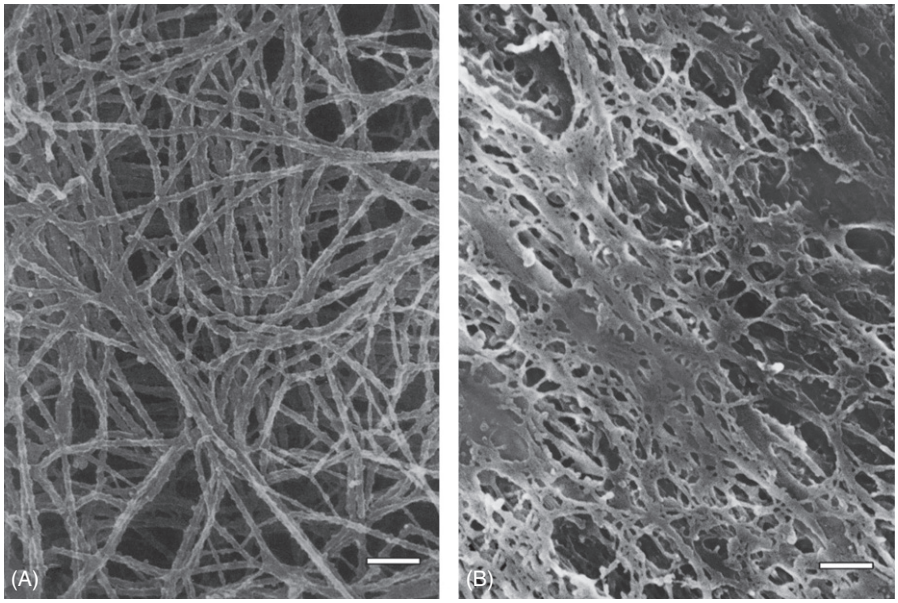

Fig. 7 SEM micrographs of subepidermal ECM observed in the cryo-SEM at −168°C following (A) standard chemical fixation and (B) cryofixation. (A) standard chemical fixation, followed by plunge-freezing and freeze-drying. Collagen fibrils form a random network with large empty spaces and are decorated with only few granular precipitates. (B) Direct plunge-freezing and freeze-drying. Collagen fibrils are densely covered with precipitates and form a dense, even matrix with numerous small clefts. Scale bars: 0.2 µm. Reprinted with permission from Epperlein et al. (1997).

of repeating disaccharides of glucuronic acid and *N*-acetylglucosamine. The number of disaccharide repeats can be 10,000 or more, and thus reach 10 µm if stretched (Hascall and Laurent, 1997). HA forms highly hydrated randomly kinked coils in solution and starts to entangle at concentrations of less than 1 mg/ml (Laurent *et al*., 1996). Within the matrices of the ECM, HA mainly interacts with proteoglycans via linker proteins. At cell surfaces it binds with hyaluronan-binding proteins (HABPs), such as CD44 and RHAMM (Reichardt, 1993; Toole, 2004). It is present predominantly in the epidermis and dermis of the skin (Hascall and Laurent, 1997), and also, for example, in the vitreous of the eye, in the rooster comb, or in Wharton's jelly of the umbilical cord (Scott *et al*., 1991). HA is involved in the control of cell proliferation, NC and tumor cell migration, wound repair, and various physiological processes (Chen and Abatangelo, 1999; Hayen *et al*., 1999; Whight *et al*., 1991). Furthermore, it plays a role in tumorigenesis, signal transduction, multidrug resistance, and angiogenesis (Toole, 2004).

The molecular model of HA in solution is not clear because it partially relies on TEM observations of HA solutions (Scott *et al*., 1991) that were not optimally freeze-dried. According to these observations, HA is a network-forming polymer with the ability to form 3D honeycomb-like structures. A more recent characterization describes HA

molecules in solution as expanded random coils that may form networks with pores that continuously change in size (Hascall and Laurent, 1997). Because the appearance of HA in natural biological samples may be different from such theoretical models based on HA in solution, the fibrillar networks (Whight *et al*., 1991), honey-comb-like structures (Scott *et al*., 1991), or porous networks (Hascall and Laurent, 1997) observed may be due to segregation patterns obtained by fixation artifacts during standard chemical fixation and/or ice crystal formation during cryofixation. In this paragraph we use various cryofixation protocols to demonstrate the structure of HA in axolotl embryos (stage 35) with TEM immunohistochemistry of HABP (Fig. 8). When the cryofixed embryonic axolotl ECM is labeled with HABP, the structural preservation of HA appears less regular (Figs. 8D,D', with UA; Figs. 8E,E', without UA) than after standard chemical fixation and freeze-substitution (Fig. 8C,C') where HA seems to predominate in honeycomb-like patterns, especially when the images are compared at higher magnification. Thus, at present, our TEM observations reveal a less regular honeycomb-like pattern (Figs. 8E and E') as the optimal result for the structure of natural HA in the subepidermal ECM of axolotl embryos (stage 35) following HPF/FS, fixation with 0.05% GA, no UA, and HABP immunohistochemistry (Epperlein *et al*., 2000a). In addition, the labeling efficiency is much better after HPF (Figs. 8E,E') than after chemical fixation (Figs. 8C, C').

a. Standard Chemical Fixation (PFA/GA) and Freeze-Substitution (FS) Excised trunks of axolotl embryos (stages 33–35) were chemically fixed in 4% PFA in 0.1 M phosphate buffer at pH 7.4 overnight at 4°C. The tissue blocks were then infiltrated with 2.3 M sucrose overnight, frozen in liquid nitrogen, and freeze-substituted (FS) in a Leica AFS device, in pure methanol for 70 h at −80°C, followed by infiltration with Lowicryl HM20 and UV polymerization at −35°C (See Fig. 8C)

b. High-Pressure Freezing (HPF) Small pieces of dorsolateral trunk epidermis (length 2 mm, width 1 mm), including subepidermal ECM of embryos at stages 33–35, are excised with tungsten needles, transferred to cryoprotectants (a mixture of 10% polyvinyl pyrrolidone and 7% methanol in 0.1 M potassium–phosphate buffer; Epperlein *et al*., 1997), and placed between two cylindrical aluminum platelets that form a double cup with a cavity of 200 µm depth. The tissue samples are then frozen with a high-pressure freezer (BAL-TEC HPM 010, Balzers, Liechtenstein). The platelets are carefully opened under liquid nitrogen and transferred to 2-ml microtubes with screw caps containing the precooled (–90°C) substitution medium consisting of 0.05% glutaraldehyde in acetone either with (Figs. 8D and D') or without (Figs. 8E and E') 0.5% uranyl acetate. The samples are freeze-substituted for 24 h at −90°C, 4 h at −60°C, and 3 h at −30°C in a freeze-substitution device (Bal-Tec FSU 010), washed with pure ethanol at −30°C, and infiltrated with ethanol/HM20. Embedding in Lowicryl HM20 and UV polymerization is performed at −35°C.

c. TEM Immunocytochemistry with HABP Ultrathin sections (70 nm) through conventionally fixed, or HPF-frozen samples (embryos at stages 33–35) embedded in

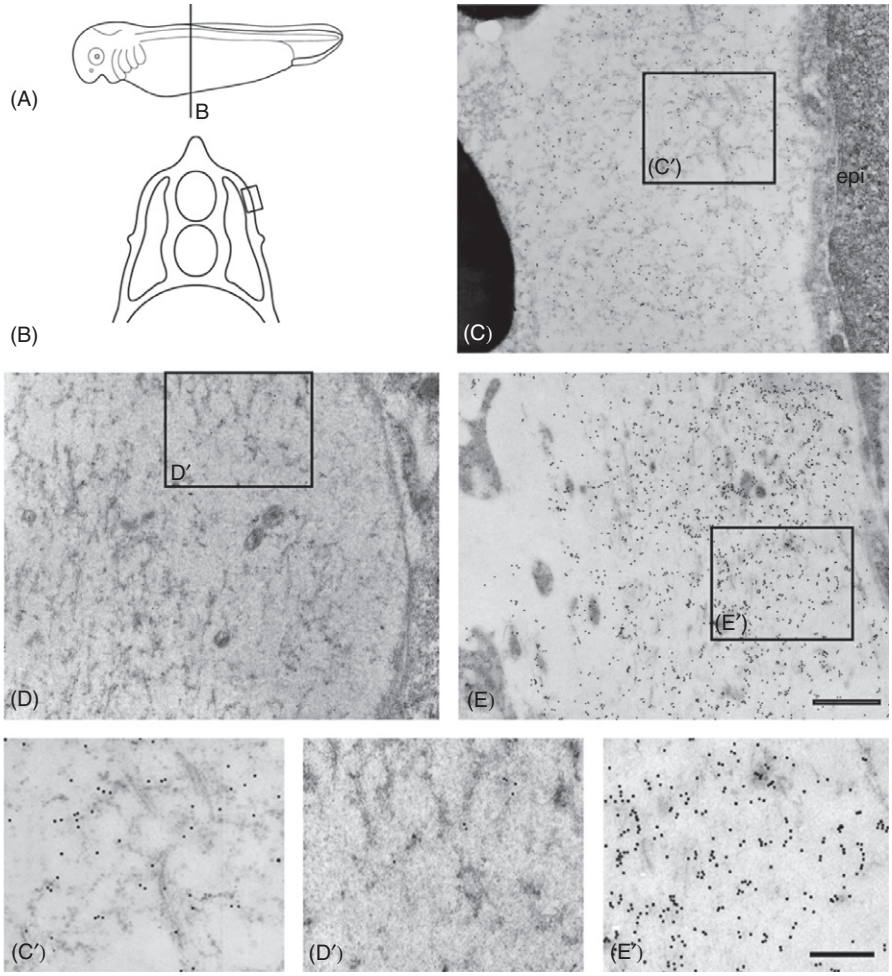

Fig. 8 Post-embedding TEM labeling of hyaluronan with HABP on ultrathin Lowicryl (HM20) sections through trunk epidermis/subepidermal ECM of dark (D/d) axolotl embryos. (A) Schematic drawing of an axolotl embryo at stage 35. The trunk level of subepidermal ECM is boxed. (B) Schematic transverse section through mid trunk area marked in A with inset indicating ECM areas displayed in C–D. (C) Fixation with 4% PFA, freeze-substitution in methanol, no *en bloc* staining with UA. The ECM is evenly labeled, its material present predominantly as "honeycomb"-like nets. (D) Fixation by HPF, freeze-substitution in acetone containing 0.05% GA and 0.5% UA. The ECM is visible as flocculent, irregular net-like and fibrillar material. The labeling intensity is very low. (E) Fixation by HPF, freeze-substitution in acetone containing 0.05% GA, no UA. The ECM appears as flocculent material, forming less regular honeycomb-like nets and fibrils than in C. Strong labeling with HABP. The contrast of cell and matrix structures is lower than in D due to the lack of UA. (C'–E') show framed regions in C–E at higher magnification. Scale bars: 1 µm (C–E), 0.5 µm (C'–E').

Lowicryl HM20, are blocked with PBS containing 0.2% gelatin. The samples are incubated with biotinylated HABP (1:1000) overnight at 4°C in PBS/gelatin. After washing with PBS/gelatin, the samples are incubated with rabbit–anti-biotin antibodies (1:50 in PBS/gelatin) for 1 h at room temperature. Washing in PBS/gelatin follows. The samples are incubated with a 10-nm gold-coupled goat anti-rabbit-IgG for 2 h at room temperature. After washing with PBS/gelatin, PBS and water samples are poststained with aqueous uranyl acetate and lead citrate according to standard protocols prior to investigation.

IV. Materials

- **Embryo culture media:** For *Xenopus*: MBSH (88 mM NaCl, 1 mM KCl, 2.4 mM $NaHCO_3$, 0.82 mM $MgSO_4$, 0.41 mM $CaCl_2$, 0.33 mM $Ca(NO_3)_2$, 10 mM HEPES pH 7.4; 10 mg/ml streptomycinsulfate and penicillin. For *Ambystoma*: Steinberg solution, 1000 ml (Steinberg, 1957): *Solution A*: 3.4 g NaCl, 0.05 g KCl, 0.205 g $MgSO_4 \times 7$ H2O, 4 ml 1 N HCl (about 9 ml 1N HCl in 100 ml aqua bidest), 0.56 g TRIS (Sigma) and 900 ml aqua bidest; plus *Solution B*: 0.08 g $Ca(NO_3)_2 \times 4H_2O$ and 100 ml aqua bidest.
- **Fixatives:** For ultrastructure/SEM: Modified Karnovsky's fixative (Karnovsky, 1965): 2.5% glutaraldehyde (GA), and 2% paraformaldehyde (PFA) in either 50 mM HEPES or in 0.1 M phosphate buffer, or modified Karnovsky's fixative containing 1.5% GA +1.5% PFA when RR, CPC, or tannic acid was added for precipitating ECM material. Secondary fixative: 1% OsO_4 in 0.1 M cacodylate buffer or PBS. For immunocytochemistry: 4% paraformaldehyde ±0.1% glutaraldehyde in 0.1 M phosphate buffer.
- **Embedding media**: For light microscopy: Technovit 7100 (Heraeus-Kulzer). For TEM: Spurr's resin kit (EMS # 14300), Epon 812 or EMbed-812 kit (EMS, # 14120), Lowicryl K4M kit (EMS # 14330) or HM20 kit (EMS # 14340).
- **Chemicals:** BSA (Merck, # 1.12018), gelatin (local food brand), glutaraldehyde (25% in water, EMS # 16220), HEPES (EMS # 16782), lead citrate (EMS # 17810), low-melting-point agarose (e.g., Sigma A9414), methyl cellulose (25 centipoises, Sigma M-6385), OsO_4 (4% in water, EMS # 19170), paraformaldehyde (granular, EMS # 19208), sucrose (EMS # 21600), uranyl acetate (Polysciences # 21447).
- **Secondary antibodies and detection systems:** We use Alexa488- and Alexa555-conjugated secondary antibodies for immunofluorescence, DAPI (Invitrogen) as a counterstain and ProLong Gold (Invitrogen P36930) as mounting medium. For EM, we use protein A conjugated to 10-nm or 15-nm gold particles (Aurion). Alternatively, secondary antibodies conjugated to gold particles from several companies (Aurion, Jackson ImmunoResearch, British Biocell) can be used. Ultrasmall gold-conjugated antibodies are purchased from EMS/Aurion as well as the R-Gent-SE-EM silver enhancement kit (EMS/Aurion # 25521)
- **Tools and materials:** Flat embedding mold (EMS # 70901), lockable double grids (type 50/50, Embra, The Netherlands), microtubes with screw cap (Sarstedt #72.694),

perfect loop (Plano), pins for cryo-sectioning (Leica specimen carrier # 16701950), polylysin-coated microscope slides (Menzel/VWR # 631-1349), slide embedding mold (EMS # 70172), water-repellent silicon pen (Pap-pen, Plano # 22304).

V. Discussion and Outlook

For more than a century, amphibian embryos have been classic models in cell and developmental biology. They were at the forefront of biological sciences in the early 20th century, culminating in the most influential organizer experiment (Spemann and Mangold, 1924). However, for more than 50 years the molecular nature of many discovered processes remained mysterious. Many researchers switched to models, such as *Drosophila* or the zebrafish that seemed to be more suitable for genetic analysis. Only after the discovery and characterization of the first organizer genes, and different embryonic inducers, embryology of amphibians has regained interest and is now successfully combined with molecular biology. Many long-standing developmental puzzles were solved over the past 20 years (De Robertis, 2009; Heasman, 2006; Kimelman, 2006). A plethora of developmental regulators, such as adhesion molecules and signal molecules, receptors, or transcription factors, has been discovered in many different screens where embryonic assays were combined with molecular biology. Various roles of such factors during development are currently being studied. A deeper understanding of the cell biological functions of these factors can, however, only be achieved if their subcellular distribution and trafficking are known, as well as their interaction with other proteins and their involvement in different subcellular processes. In some cases, cell biological processes can only be analyzed by ultrastructural analysis in the electron microscope. In particular, the correlation of fluorescent signals detected at the light microscopical level with subcellular structures, observed in the TEM, is a demanding task. Therefore, preparation methods for correlative LM/EM of amphibian embryos (mainly *Xenopus* and *Ambystoma*) are necessary.

Most of the protocols described here include chemical fixation and, for *Xenopus* embryos, embedding into Spurr's resin. This approach is generally considered "second best" if compared to high-pressure freezing followed by freeze-substitution and Epon embedding (McDonald, 2007; Moor, 1987). Furthermore, early *Xenopus* embryos are immunolabeled prior to embedding (i.e., pre-embedding labeling), which yields only poor ultrastructural preservation compared to post-embedding labeling (Kurth, 2003; Schwarz and Humbel, 2007). For amphibian embryos, these protocols generally still provide the best compromise for obtaining reasonable ultrastructural data. In the future, the systematic adaptation of additional approaches, such as cryopreparation techniques (HPF, Tokuyasu), or microwave-assisted processing, might help to further analyze many cell biological processes in amphibian embryos.

A. Chemical Fixation vs. HPF

High-pressure freezing followed by freeze-substitution is considered the "gold standard" for obtaining optimal ultrastructural preservation of cells and tissues (Moor, 1987; Studer *et al*., 2001, McDonald, 2007) and was recently successfully applied to adult *Xenopus* tissues (Van Herp *et al*., 2005; Wang *et al*., 2005). However, for optimal freezing results, a specimen should not be thicker than 0.2 mm (Studer *et al*., 2008). *Xenopus* eggs and early embryos are spheres of about 1–1.3 mm in diameter, axolotl eggs about 2 mm. Therefore, only parts of embryos, such as tissue explants or isolated cells, can be frozen successfully. The ECM preparations presented in Figs. 7 and 8 demonstrate that, in such cases, ultrarapid freezing is an attractive option.

Explants and isolated cells are important models for many early developmental processes (e.g., the animal cap assay or Keller explants for the analysis of convergent extension, cultivation of isolated embryonic cells, or organ anlagen, Sive *et al*., 2000). Those explants and cells in culture might be quite suitable for HPF. Alternatively, chemical fixation might be improved with microwave-assisted fixation protocols, using either the microwave device from Ted Pella (Milestone rapid electron microscopy (REM) histoprocessor) or the Leica microwave-based tissue processor (Leica EM AMW, for examples, see Schroeder *et al*., 2006). To our knowledge, this has not been tried for amphibian embryos so far. The application and/or combination of HPF and microwave fixation/processing might be a promising option for future experiments (see also Chapter 18 by Webb/Parton, this volume).

B. Spurr's Resin As an Embedding Medium

The use of Spurr's resin as an embedding medium leads to stronger extraction compared with Epon. For early *Xenopus* and axolotl embryos, however, a low-viscosity resin proved to be essential because of the massive amount of intracellular yolk granules and the problems caused by them during infiltration and sectioning (Kurth, 2003; Müller and Hausen, 1995). Again, the microwave option might help to improve resin infiltration and offer the possibility to switch from Spurr's to Epon as an embedding medium.

C. On Section Labeling vs. Pre-Embedding Labeling

On-section labeling of resin sections is an effective method for many cells and tissues, although the labeling efficiency is relatively poor (Fig. 2; Kurth *et al*., 1996; Schwarz and Humbel, 2007). Proteins that are easy to detect in adult tissues, however, might be below the detection limit in embryonic tissues with this method, whereas pre-embedding labeling at the light microscopical level leads to strong staining of the same proteins (Kurth, 2003). Staining of cryosections after Tokuyasu is more sensitive (Schwarz and Humbel, 2009; Slot and Geuze, 2007) and might offer an alternative approach for analyzing subcellular protein distribution even in the amphibian embryo. To our knowledge, the staining of ZO-1 (Fig. 3) is the first demonstration of this

technique in a *Xenopus* embryo. Unfortunately, amphibian blastula or gastrula stages are extremely difficult to cut at low temperatures. In such cases, the whole-mount staining of thick vibratome sections in combination with nanogold-coupled markers and silver enhancement currently reveals the best compromise between preservation of ultrastructure and antigenicity (Fig. 4; Kurth, 2003).

Acknowledgments

The authors would like to thank Inge Zimmermann, and Metta Riebesell for excellent technical assistance, and E.M. Tanaka for the kind donation of reagents.

References

Akey, C. W., and Radermacher, M. (1993). Architecture of the *Xenopus* nuclear pore complex revealed by three-dimensional cryo-electron microscopy. *J. Cell Biol*. **122**, 1–19.

Allen, T. D., Rutherford, S. A., Murray, S., Sanderson, H. S., Gardiner, F., Kiseleva, E., Goldberg, M. W., and Drummond, S. P. (2007a). A protocol for isolating *Xenopus* oocyte nuclear envelope for visualization and characterization by scanning electron microscopy (SEM) or transmission electron microscopy (TEM. *Nat. Protoc*. **2**, 1166–1172.

Allen, T. D., Rutherford, S. A., Murray, S., Sanderson, H. S., Gardiner, F., Kiseleva, E., Goldberg, M. W., and Drummond, S. P. (2007b). Generation of cell-free extracts of *Xenopus* eggs and demembranated sperm chromatin for the assembly and isolation of in vitro-formed nuclei for western blotting and scanning electron microscopy (SEM). *Nat. Protoc*. **2**, 1173–1179.

Amaya, E., Offield, M. F., and Grainger, R. M. (1998). Frog genetics: *Xenopus tropicalis* jumps into the future. *Trends Genet*. **14**, 253–255.

Armstrong, J. B., and Graveson, A. C. (1988). Progressive patterning precedes somite segmentation in the Mexican axolotl (*Ambystoma mexicanum*). *Dev. Biol*. **126**, 1–6.

Bordzilovskaya, N. P., Dettlaff, T. A., Duhon, S. T., and Malacinski, G. M. (1989). Developmental-stage series of axolotl embryos. *In* "Developmental Biology of the Axolotl*"* (J. B. Armstrong, and G. M. Malacinski, eds.) pp. 201–219. Oxford University Press, NY.

Cardellini, P., Cirelli, A., and Citi, S. (2007). Tight junction formation in early *Xenopus laevis* embryos: Identification and ultrastructural characterization of junctional crests and junctional vesicles. *Cell Tissue Res*. **330**, 247–256.

Cerny, R., Meulemans, D., Berger, J., Wilsch-Bräuninger, M., Kurth, T., Bronner-Fraser, M., and Epperlein, H.-H. (2004). Combined intrinsic and extrinsic influences pattern cranial neural crest migration and pharyngeal arch morphogenesis in axolotl. *Dev. Biol*. **266**, 252–269.

Chen, W. Y., and Abatangelo, G. (1999). Functions of hyaluronan in wound repair. *Wound Repair Regen*. **7**, 79–89.

Cho, K. W.Y., Blumberg, B., Steinbeisser, H., and De Robertis, E. M. (1991). Molecular nature of Spemann's organizer: The role of the *Xenopus* homeobox gene goosecoid. *Cell* **67**, 1111–1120.

Coughlin, M., Brieher, W. M., and Ohi, R. (2007). Cell-free extract systems and the cytoskeleton: Preparation of biochemical experiments for transmission electron microscopy. *Methods Mol. Biol*. **369**, 199–212.

Crane, R. F., and Ruderman, J. V. (2006). Using *Xenopus* oocyte extracts to study signal transduction. *Methods Mol. Biol*. **322**, 435–443.

Cross, M. K., and Powers, M. A. (2009). Learning about cancer from frogs: Analysis of mitotic spindles in *Xenopus* egg extracts. *Dis. Model Mech*. **2**, 541–547.

Danilchik, M. V., Bedrick, S. D., Brown, E. E., and Ray, K. (2003). Furrow microtubules and localized exocytosis in cleaving *Xenopus laevis* embryos. *J. Cell. Sci*. **116**, 273–283.

Danilchik, M. V., and Brown, E. E. (2008). Membrane dynamics of cleavage furrow closure in *Xenopus laevis*. *Dev. Dyn* **237**, 565–579.

Danscher, G. (1981). Localization of gold in biological tissue. *Histochemistry* **71**, 1–16.

De Calisto, J., Araya, C., Marchant, L., Riaz, C. F., and Mayor, R. (2005). Essential role of non-canonical wnt signalling in neural crest migration. *Development* **132**, 2587–2597.

De Robertis, E. M. (2009). Spemann's organizer and the self-regulation of embryonic fields. *Mech. Dev.* **126**, 925–941.

Epperlein, H.-H., and Löfberg, J. (1990). The development of the larval pigment patterns in *Triturus alpestris* and *Ambystoma mexicanum*. *Adv. Anat. Embryol. Cell. Biol*. **118**, 1–99.

Epperlein, H. H., Meulemans, D., Bronner-Fraser, M., Steinbeisser, H., and Selleck, M. (2000b). Analysis of cranial neural crest migratory pathways in axolotl using cell markers and transplantation. *Development* **127**, 2751–2761.

Epperlein, H.-H., Radomski, N., Wonka, F., Walther, P., Wilsch, M., Müller, M., and Schwarz, H. (2000a). Immunohistochemical demonstration of hyaluronan and its possible involvement in axolotl neural crest cell migration. *J. Struct. Biol*. **132**, 19–32.

Epperlein, H.-H., Schwarz, H., Piendl, T., Löfberg, J., Studer, D., Spring, H., and Müller, M. (1997). Improved preservation of the subepidermal extracellular matrix in axolotl embryos using electron microscopical techniques based on cryoimmobilization. *J. Struct. Biol*. **118**, 43–61.

Epperlein, H.-H., Selleck, M. A., Meulemans, D., Mchedlishvili, L., Cerny, R., Sobkow, L., and Bronner-Fraser, M. (2007). Migratory patterns and developmental potential of trunk neural crest cells in the axolotl embryo. *Dev. Dyn*. **236**, 389–403.

Falck, P., Hanken, J., and Olsson, L. (2002). Cranial neural crest emergence and migration in the Mexican axolotl (*Ambystoma mexicanum*). *Zoology* **105**, 195–2002.

Fesenko, I., Kurth, T., Sheth, B., Fleming, T. P., Citi, S., and Hausen, P. (2000). Tight juntion biogenesis in the early *Xenopus* embryo. *Mech. Dev.* **96**, 51–65.

Fey, J., and Hausen, P. (1990). Appearance and distribution of laminin during development of *Xenopus laevis*. *Differentiation* **42**, 144–152.

Gajewski, A., and Krohne, G. (1999). Subcellular distribution of the *Xenopus* p58/lamin B receptor in oocytes and eggs. *J. Cell. Sci*. **112**, 2583–2596.

Giacomello, E., Vallin, J., Morali, O., Coulter, J. S., Boulekbache, H., Thiery, J. P., and Broders, F. (2002). Type I cadherins are required for differentiation and coordinated rotation in *Xenopus laevis* somitogenesis. *Int. J. Dev. Biol*. **46**, 785–792.

Gillespie, L. L., Armstrong, J. B., and Steinberg, M. S. (1985). Experimental evidence for a proteinaceous presegmental wave required for morphogenesis of axolotl mesoderm. *Dev. Biol.* **107**, 220–226.

Goldberg, M. W., Huttenlauch, I., Hutchison, C. J., and Stick, R. (2008). Filaments made from A- and B-type lamins differ in structure and organization. *J. Cell. Sci*. **121**, 215–225.

Griffith, J. M., and Posthuma, G. (2002). A reliable and convenient method to store ultrathin thawed cryosections prior to immunolabeling. *J. Histochem. Cytochem*. **50**, 57–62.

Griffiths, G., McDowall, A., Back, R., and Dubochet, J. (1984). On the preparation of cryosections for immunocytochemistry. *J Ultrastruct. Res*. **89**, 65–78.

Gurdon, J. B., Laskey, R. A., and Reeves, O. R. (1975). The developmental capacity of nuclei transplanted from keratinized cells of adult frogs. *J. Emryol. Exp. Morphol*. **34**, 93–112.

Habermann, B., Bebin, A. G., Herklotz, S., Volkmer, M., Eckelt, K., Pehlke, K., Epperlein, H.-H., Schackert, H. K., Wiebe, G., and Tanaka, E. M. (2004). An *Ambystoma mexicanum* EST sequencing project: Analysis of 17,352 expressed sequence tags from embryonic and regenerating blastema cDNA libraries. *Genome Biol*. **5**, R67.

Hall, B. K., and Hörstadius, S. (1988). "The Neural Crest." Oxford University Press, London.

Hamburger, V. (1988). "The Heritage of Experimental Embryology." Oxford University Press, London.

Hardin, J. D., and Keller, R. E. (1988). The behaviour and function of bottle cells during gastrulation of *Xenopus laevis*. *Development* **103**, 211–230.

Hascall, V. C., and Laurent, T. (1997). Hyaluronan: Structure and physical properties. Science of hyaluronan today (online), http://www.glycoforum.gr.jp/science/hyaluronan/HA01/HA01E.html (1997).

Hausen, P., and Riebesell, M. (1991). "The Early Development of *Xenopus Laevis*. An Atlas of the Histology." Springer-Verlag, Berlin.

Hayen, W., Goebeler, M., Kumar, S., Riessen, R., and Nehls, V. (1999). Hyaluronan stimulates tumor cell migration by modulating the fibrin fiber architecture. *J. Cell. Sci*. **112**, 2241–2251.

Heasman, J. (2006). Patterning the early *Xenopus* embryo. *Development* **133**, 1205–1217.

Heasman, J., Kofron, M., and Wylie, C. (2000). Beta-catenin signaling activity dissected in the early *Xenopus* embryo: A novel antisense approach. *Dev. Biol*. **222**, 124–134.

Hess, K., Steinbeisser, H., Kurth, T., and Epperlein, H.-H. (2008). Bone morphogenetic protein-4 and noggin signaling regulates pigment cell distribution in the axolotl trunk. *Differentiation* **76**, 206–218.

Kalt, M. R. (1971). The relationship between cleavge and blastocoel formation in *Xenopus laevis*. II. Electron microscopic observations. *J. Embryol. Exp. Morphol*. **26**, 51–66.

Kalt, M. R., and Tandler, B. (1971). A study of fixation of early amphibian embryos for electron microscopy. *J. Ultrastruct. Res*. **36**, 633–645.

Karnovsky, M. J. (1965). A formaldehyde–glutaraldehyde fixative of high osmolarity for use in electron microscopy. *J. Cell Biol*. **27**, 137A.

Keller, R. E. (1980). The cellular basis of epiboly: An SEM study of deep-cell rearrangement during gastrulation in *Xenopus laevis*. *J. Embryol. Exp. Morphol*. **60**, 201–234.

Keller, R. E. (1981). An experimental analysis of the role of bottle cells and the deep marginal zone in gastrulation of *Xenopus laevis*. *J. Exp. Zool*. **216**, 81–101.

Keller, R., Davidson, L. A., and Shook, D. R. (2003). How we are shaped: The biomechanics of gastrulation. *Differentiation* **71**, 171–205.

Kimelman, D. (2006). Mesoderm induction: From caps to chips. *Nat. Rev. Genet*. **7**, 360–372.

Kragl, M., Knapp, D., Nacu, E., Khattak, S., Maden, M., Epperlein, H. H., and Tanaka, E. M. (2009). Cells keep a memory of their tissue origin during axolotl limb regeneration. *Nature* **460**, 60–65.

Kurth, T. (2003). Immunocytochemistry of the amphibian embryo – from overview to ultrastructure. *Int. J. Dev. Biol*. **47**, 373–383.

Kurth, T., Fesenko, I. V., Schneider, S., Münchberg, F. E., Joos, T. O., Spieker, T. P., and Hausen, P. (1999). Immunocytochemical studies of the interactions of cadherins and catenins in the early *Xenopus* embryo. *Dev. Dyn*. **215**, 155–169.

Kurth, T., and Hausen, P. (2000). Bottle cell formation in relation to mesodermal patterning in the *Xenopus* embryo. *Mech. Dev*. **97**, 117–131.

Kurth, T., Schwarz, H., Schneider, S., and Hausen, P. (1996). Fine structural immunocytochemistry of catenins in amphibian and mammalian muscle. *Cell Tissue Res*. **286**, 1–12.

Lah, J. J., Hayes, D. M., and Burry, R. W. (1990). A neutral pH silver development method for the visualization of 1-nanometer gold particles in pre-embedding electron microscopic immunocytochemistry. *J. Histochem. Cytochem*. **38**, 503–508.

Laurent, T. C., Laurent, U. B., and Fraser, J. R. (1996). The structure and function of hyaluronan: An overview. *Immunol. Cell Biol*. **74**, 1–7.

Le Douarin, N. M., and Kalcheim, C. (1999). "The Neural Crest." 2nd edn, Cambridge University Press, Cambridge.

Lee, J.-Y., and Harland, R. M. (2007). Actomyosin contractility and microtubules drive apical constriction in *Xenopus* bottle cells. *Dev. Biol*. **311**, 40–52.

Löfberg, J., Nynäs-McCoy, A., Olsson, C., Jönsson, L., and Perris, R. (1985). Stimulation of initial neural crest cell migration in the axolotl embryo by tissue grafts and extracellular matrix transplanted on microcarriers. *Dev. Biol*. **107**, 442–459.

Löfberg, J., Perris, R., and Epperlein, H.-H. (1989a). Timing in the regulation of neural crest cell migration: Retarded "maturation" of regional extracellular matrix inhibits pigment cell migration in embryos of the white axolotl mutant. *Dev. Biol*. **131**, 168–181.

Löfberg, J., Epperlein, H. H., Perris, R., and Stigson, M. (1989b). Neural crest cell migration: A pictorial essay. In: Developmental biology of the axolotl (Armstrong, J. B. and Malacinsky, G. M., eds.), Oxford University Press, New York.

Lourim, D., and Krohne, G. (1993). Membrane-associated lamins in *Xenopus* egg extracts: Identification of two vesicle populations. *J. Cell Biol*. **123**, 501–512.

Luft, J. H. (1971a). Ruthenium red and violet. I. Chemistry, purification, methods of use for electron microscopy and mechanism of action. *Anat. Rec*. **171**, 347–368.

Luft, J. H., (1971b). Ruthenium red and violet. II. Fine structural localization in animal tissues. *Anat. Rec*. **171**, 369–415.

Maco, B., Fahrenkrog, B., Huang, N. P., and Aebi, U. (2006). Nuclear pore complex structure and plasticity revealed by electron and atomic force microscopy. *Methods Mol. Biol*. **322**, 273–288.

Mandato, C. A., Weber, K. L., Zandy, A. J., Keating, T. J., and Bement, W. M. (2001). *Xenopus* egg extract as a model system for analysis of microtubule, actin filament, and intermediate filament interactions. *Methods Mol. Biol*. **161**, 229–239.

Maresca, T. J., and Heald, R. (2006). Methods for studying spindle assembly and chromosome condensation in *Xenopus* egg extracts. *Methods Mol. Biol*. **322**, 459–474.

McDonald, K. (2007). Cryopreparation methods for electron microscopy of selected model systems. *Methods Cell Biol*. **79**, 23–56.

Mchedlishvili, L., Epperlein, H. H., Telzerow, A., and Tanaka, E. M. (2007). A clonal analysis of neural progenitors during axolotl spinal cord regeneration reveals evidence for both spatially restricted and multipotent progenitors. *Development* **134**, 2083–2093.

Merzdorf, C. S., Chen, Y. H., and Goodenough, D. A. (1998). Formation of functional tight junctions in *Xenopus* embryos. *Dev. Biol*. **195**, 187–203.

Miltner, M. J., and Armstrong, J. B. (1983). Spermatogeneis in the Mexican axolotl, *Ambystoma mexicanum*. *J. Exp. Zool*. **227**, 255–263.

Moor, H. (1987). Theory and practice of high-pressure freezing. *In* "Cryotechniques in Biological Electron Microscopy" (Steinbrecht, R. A., Zierold, K., eds.) 175–191. Springer, Berlin, Germany.

Moriya, N., Komazaki, S., Takahashi, S., Yokota, C., and Asashima, M. (2000). In vitro pancreas formation from *Xenopus* ectoderm treated with activin and retinoic acid. *Dev. Growth Differ*. **42**, 593–602.

Müller, H. A., and Hausen, P. (1995). Epithelial cell polarity in early *Xenopus* development. *Dev. Dyn*. **202**, 405–420.

Nakatsuji, N., Smolira, M. A., and Wylie, C. C. (1985). Fibronectin is visualized by scanning electron microscopy immnuocytochemistry on the substratum for cell migration in *Xenopus laevis* gastrulae. *Dev. Biol*. **107**, 264–268.

Nieuwkoop, P. D., and Faber, J. (1967). "Normal Table of *Xenopus laevis* (Daudin)." North-Holland, Amsterdam.

Nye, H. L., Cameron, J. A., Chernoff, E. A., and Stocum, D. L. (2003). Extending the table of stages of normal development of the axolotl: Limb development. *Dev. Dyn*. **226**, 555–560.

Olsson, L., Stigson, M., Perris, R., Sorrell, J. M., and Löfberg, J. (1996a). Distribution of keratan sulphate and chondroitin sulphate in wild type and white mutant axolotl embryos during neural crest cell migration. *Pigment Cell Res*. **9**, 5–17.

Olsson, L., Svensson, K., and Perris, R. (1996b). Effects of extracellular matrix molecules on subepidermal neural crest cell migration in wild type and white mutant (dd) axolotl embryos. *Pigment Cell Res*. **9**, 18–27.

Osafune, K., Nishinakamura, R., Komazaki, S., and Asashima, M. (2002). In vitro induction of the pronephric duct in *Xenopus* explants. *Dev. Growth Differ*. **44**, 161–167.

Perris, R., Löfberg, J. ,, Fällström, C., von Boxberg, Y., Olsson, L., and Newgreen, D. F. (1990). Structural and compositional divergencies in the extracellular matrix encountered by neural crest cells in the white mutant axolotl embryo. *Development* **109**, 533–551.

Putta, S., Smith, J. J., Walker, J. A., Rondet, M., Weisrock, D. W., Monaghan, J., Samuels, A. K., Kump, K., King, D. C., Maness, N. J., Habermann, B., Tanaka, E., et al., (2004). From biomedicine to natural history research: EST resources for ambystomatid salamanders. *BMC Genomics* **5**, 54.

Reichardt, L. F. (1993). Extracellular molecules and their receptors. *In* "Guide Book to the Extracellular Matrix and Adhesion Proteins" (Kreis, T., and Vale, R. (eds.)) pp. 3–11. Oxford University Press, Oxford, London.

Reintsch, W. E., and Hausen, P. (2001). Dorsoventral differences in cell–cell interactions modulate the motile behaviour of cells from the *Xenopus* gastrula. *Dev. Biol*. **240**, 387–403.

Sadaghiani, B., and Thiebaud, C. H. (1987). Neural crest development in the *Xenopus laevis* embryo, studied by interspecific transplantation and scanning electron microscopy. *Dev. Biol*. **124**, 91–110.

Schneider, S., Steinbeisser, H., Warga, R. M., and Hausen, P. (1996). Beta-Catenin translocation into nuclei demarcates the dorsalizing centers in frog and fish embryos. *Mech. Dev*. **57**, 191–198.

Schroeder, T. E. (1970). Neurulation in *Xenopus laevis*. An analysis and model based upon light and electron microscopy. *J. Embryol. Exp. Morphol*. **23**, 427–462.

Schroeder, J. A., Gelderblom, H. R., Hauroeder, B., Schmetz, C., Milios, J., and Hofstaedter, F. (2006). Microwave-assisted tissue processing for same-day-EM-diagnosis of potential bioterrorism and clinical samples. *Micron* **37**, 577–590.

Schwab, M. S., Gossweiler, U., and Dreyer, C. (1998). Subcellular distribution of distinct nucleolin subfractions recognized by two monoclonal antibodies. *Exp. Cell Res*. **239**, 226–234.

Schwarz, H., and Humbel, B. (2007). Correlative light and electron microscopy using immunolabeled resin sections. *Methods Mol. Biol*. **369**, 229–256.

Schwarz, H., and Humbel, B. M. (2009). Correlative light and electron microscopy. *In* "Hand Book of Cryo-Preparation Methods for Electron Microscopy" (Cavalier, A., Spehner, D., Humbel, B. M., eds.) pp 537–565. CRC Press, Boca Raton, FL.

Scott, J. E., Cummings, C., Brass, A., and Chen, Y. (1991). Secondary and tertiary structures of hyaluronan in aqueous solution, investigated by rotary shadowing-electron microscopy and computer simulation. *Biochem. J*. **274**, 699–705.

Shook, D. R., Majer, C., and Keller, R. (2004). Pattern and morphogenesis of presumptive superficial mesoderm in two closely related species, *Xenopus laevis* and *Xenopus tropicalis*. *Dev. Biol*. **270**, 163–185.

Sive, H. L., Grainger, R. M., and Harland, R. M. (2000). Early Development of *Xenopus Laevis*: A Laboratory Manual. Cold Spring Harbor Laboratory Press, New York.

Slack, J. M.W., Lin, G., and Chen, Y. (2008). The *Xenopus* tadpole: A new model for regeneration research. *Cell Mol. Life Sci*. **65**, 54–63.

Slot, J. W., and Geuze, H. J. (2007). Cryosectioning and immunolabeling. *Nat. Protoc*. **2**, 2480–2591.

Sobkow, L., Epperlein, H. H., Herklotz, S., Straube, W. L., and Tanaka, E. M. (2006). A germline GFP transgenic axolotl and its use to track cell fate: Dual origin of the fin mesenchyme during development and the fate of blood cells during regeneration. *Dev. Biol*. **290**, 386-397.

Spemann, H., and Mangold, H. (1924). Über die Induktion von Embryonalanlagen durch Implantation artfremder Organisatoren. *W. Roux' Arch. f. Entwicklungsmech*. **100**, 599–638.

Spurr, A. R. (1969). A low viscosity epoxy resin embedding medium for electron microscopy. *J. Ultrastr. Res*. **26**, 31–43.

Steinberg, M. S. (1957). A non-nutrient culture medium for amphibian embryonic tissue. *Carnegie Inst Wash. Year B* **56**, 347–348.

Stick, R., and Schwarz, H. (1983). Disappearance and reformation of the nuclear lamina structure during specific stages of meiosis in oocytes. *Cell* **33**, 949–958.

Stierhof, Y. D. (2009). Immunolabeling of ultrathin sections with enlarged 1 nm gold or Q-dots. *In* "Hand Book of Cryo-Preparation Methods for Electron Microscopy" (Cavalier, A., Spehner, D., Humbel, B. M., eds.) pp. 587–616. CRC Press, Boca Raton, FL.

Stoffler, D., Feja, B., Fahrenkrog, B., Walz, J., Typke, D., and Aebi, U. (2003). Cryo-electron tomography provides novel insights into nuclear pore architecture: Implications for nucleocytoplasmic transport. *J. Mol. Biol*. **328**, 119–130.

Studer, D., Graber, W., Al-Amoudi, A., and Eggli, P. (2001). A new approach for cryofixation by high-pressure freezing. *J. Microsc*. **2003**, 285–294.

Studer, D., Humbel, B. M., and Chiquet, M. (2008). Electron microscopy of high pressure frozen samples: Bridging the gap between cellular ultrastructure and atomic resolution. *Histochem. Cell Biol*. **130**, 877–889.

Tammaro, P., Shimomura, K., and Proks, P. (2008). *Xenopus* oocytes as a heterologous expression system for studying ion channels with the patch-clamp technique. *Methods Mol. Biol*. **491**, 127–139.

Tokuyasu, K. T. (1976). Membranes as observed in frozen sections. *J. Ultrastruct. Res*. **55**, 281–287.

Toole, B. P. (2004). Hyaluronan: From extracellular glue to pericellular cue. *Nat. Rev. Cancer* **4**, 528–539.

Van Herp, F., Coenen, T., Geurts, H. P., Janssen, G. J., and Martens, G. J. (2005). A fast method to study the secretory activity of neuroendocrine cells at the ultrastructural level. *J. Microsc*. **218**, 79–83.

Venable, J. H., and Coggeshall, R. (1965). A simplified lead citrate stain for use in electron microscopy. *J. Cell Biol*. **25**, 407–408.

Voss, S. R., Epperlein, H. H., and Tanaka, E. M. (2009). *Ambystoma mexicanum*, the axolotl: A versatile amphibian model for regeneration, development, and evolution studies.. *Cold Spring Harb. Protoc*., doi: 10.1101/pdb.emo128.

Walther, P. (2008). High-resolution cryo-SEM allows direct identification of F-actin at the inner nuclear membrane of *xenopus* oocytes by virtue of its structural features. *J. Microsc*. **232**, 379–385.

Wang, L., Humbel, B. M., and Roubos, E. W. (2005). High-pressure freezing followed by cryosubstitution as a tool for preserving high quality ultrastructure and immunoreactivity in the *Xenopus laevis* pituitary gland. *Brain Res. Protoc*. **15**, 155–163.

Whight, T. N., Heinegard, D. K., and Hascall, V. C. (1991). Proteoglycans. *In* "Cell Biology of Extracellular Matrix" (Hay, E. D. ed.), 2nd edn., pp. 45–78. Plenum, NY.

Winklbauer, R., and Nagel, M. (1991). Directional mesoderm cell migration in the *Xenopus* gastrula. *Dev. Biol*. **148**, 573–589.

Winklbauer, R., Selchow, A., Nagel, M., and Angres, B. (1992). Cell interaction and its role in mesoderm cell migration during *Xenopus* gastrulation. *Dev. Dyn*. **195**, 290–302.

Youn, B. W., Keller, R. E., and Malacinski, G. M. (1980). An atlas of notochord and somite morphogenesis in several anuran and urodelean amphibians. *J. Embryol. Exp. Morphol*. **59**, 223–247.

Youn, B. W., and Malacinski, G. M. (1981). Somitogenesis in the amphibian *Xenopus laevis*: Scanning electron microscopic analysis of intrasomitic cellular arrangements during somite rotation. *J. Embryol. Exp. Morphol*. **64**, 23–43.

Zackson, S. L., and Steinberg, M. S. (1987). Chemotaxis or adhesion gradient? Pronephric duct elongation does not depend on distant sources of guidance information. *Dev. Biol*. **124**, 418–422.